



Report

Course Project: The assumptions underlying K41 theory and how
deterministic systems display chaos.

Name: Francesco Sala
Date: May 21, 2023
Course: Turbulence ME-467
Instructor: Tobias Schneider

1 Part I: Statistical Analysis of Turbulence

1.1 Review of the K41 theory and its assumptions

1.1.1 Remarks

The first highlighted sentence is formulated wrongly. The assumption behind the Kolmogorov theory is that, in the limit for the viscosity $\nu \rightarrow 0$, $\varepsilon(\nu) \rightarrow \varepsilon > 0$, i.e. ε is no longer a function of ν and becomes constant for $\nu \rightarrow 0$. This does not mean that the fluid behaves as an inviscid fluid: for an inviscid fluid, we would have $\varepsilon = 0$. In the K41 theory viscosity plays a role only at the smallest scales and hence the sentence "(...) the viscosity of the fluid is not significant at the smallest scale" is fallacious. The following could be a corrected version of the initial erroneous statement:

K41 theory is based on the assumption that the turbulent flow with an infinite Reynolds number has a finite nonvanishing mean rate of dissipation ε per unit mass. This assumption is based on the idea that at the smallest scales, in the limit for $\nu \rightarrow 0$, the energy dissipation, due to viscosity, becomes constant.

For what concerns the self-similarity assumption, while it is known that turbulence displays intermittency in the dissipation range, it is yet to be proved that there may be intermittency even in the inertial range. If this was to be proved, the central assumption of self-similarity may not be verified. A random function $u(t)$ is said to be intermittent if the corresponding high-pass filtered signal shows a flatness that grows unbounded with the filter cutoff frequency. In practice, the intermittency can be measured using higher order moments: if higher order moments could be easily and precisely computed, it would be possible to confirm or disprove the correctness of K41. One way of testing the reliability of K41 is given by the study and computation of the structure functions. The K41 theory predicts that the structure function of order p should follow:

$$S_p(l) = C_p \varepsilon^{p/3} l^{p/3} \quad (1)$$

Now, while the accordance of the theory with experiments for $p = 2, 3$ can be more easily verified, measurements of high-order structure functions are a complicated task since they require the measurement of high-order moments of velocity increments, which in turn require the tails of the probability distribution functions that are composed, by definition, of rare events. It would thus be necessary to process lengthy signals to be able to properly estimate such structure functions, provided that higher-order moments exist. As of today, there is no certainty about the incorrectness of the K41 theory for high-order structure functions, even though Gagne has shown that $S_6(l)$ seems not to follow the prediction ($p = 6$). If the intermittency in the inertial range were to be proved, Eq. 1 would have to be corrected, allowing S_p to be a function of both l and the integral scale l_0 , and introducing corrective exponents in the form:

$$\zeta_p = \frac{p}{3} + \alpha_p \quad (2)$$

There exist many different models to incorporate intermittency into the K41 theory. Among these, a popular model is the β -model: it is based on the fact that, at each step in the Richardson cascade, the number of smaller eddies compared to the larger ones is such that the fraction of volume occupied is decreased by a factor β . These corrective models allow adjusting the exponent $p/3$ in Eq. 1 as in Eq. 2. As of today, corrections due to intermittency are thought to be likely necessary, but there is no actual proof yet.

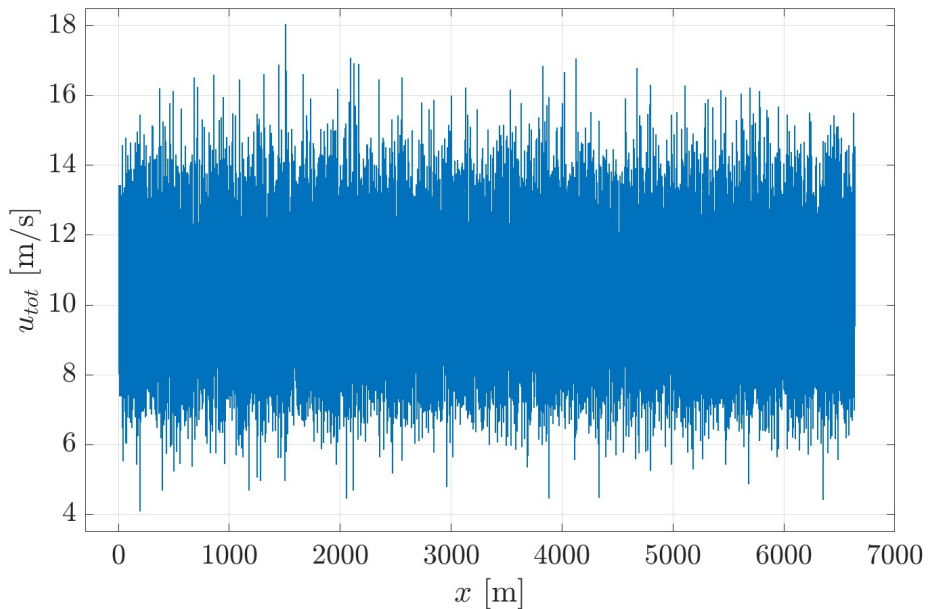
1.2 Data Analysis

In the analysis that follows, thirteen million values of velocity were taken into account, as collected by a hot wire probe of length 1 mm in the Warhaft Wind and Turbulence Tunnel at Cornell University in units of m/s. The sampling frequency was $f_s = 20 \text{ kHz}$, and the turbulence was primarily generated by randomly rotating paddles of about 100 mm in size. For all the computations that follow, a kinematic viscosity of the air ν at $T = 25^\circ\text{C}$ equal to $1.56 \times 10^{-5} \text{ m}^2/\text{s}$ was used.

1.2.1 Velocity Signal in the Spatial Domain

The given data points were obtained in the time domain, i.e. $u_{tot} = u_{tot}(t)$. If we define the velocity fluctuations u as :

$$u = u_{tot} - U \quad (3)$$



Plot A: Trend of u_{tot} against the spatial position x . All data points are displayed.

and provided that the turbulence intensity I is sufficiently small:

$$I = \frac{\sqrt{\langle u^2 \rangle}}{U} \ll 1 \quad (4)$$

Taylor's frozen flow hypothesis can be applied, leading to:

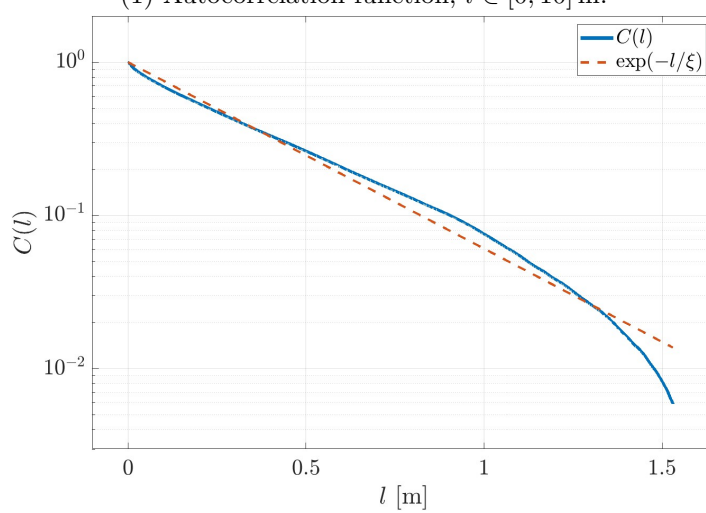
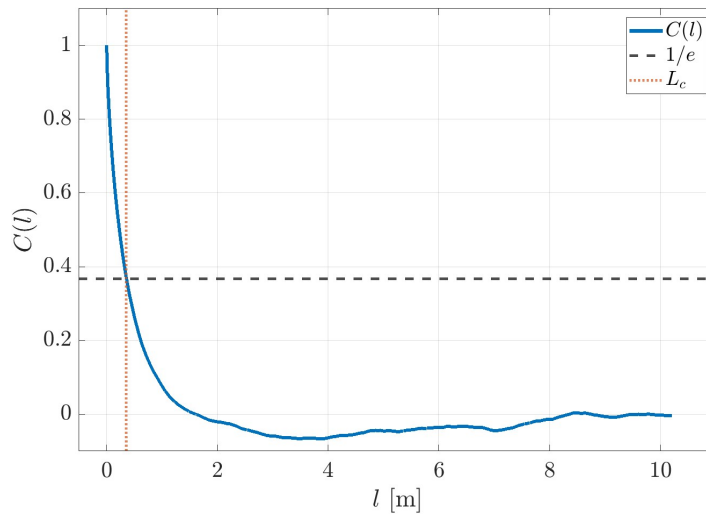
$$u_{tot}(x, t + \tau) - u_{tot}(x, t) \approx u_{tot}(x - l, t) - u_{tot}(x, t) \quad (5)$$

where $l = U\tau$. For the given data, $I = 0.1225$: we can thus apply Taylor's hypothesis. Note the minus sign in the argument of the first term in the RHS: the element of fluid that reaches the hot wire probe the sooner, will be the furthest in space when changing the domain. Given the sampling frequency f_s , the delay in time between two contiguous samples of velocity is $\tau = \frac{1}{f_s}$. Hence, the delay in space will be $l = \frac{U}{f_s}$, and a vector of spatial positions can be defined by multiplying the vector of time instants by U . In order to respect the above argument, the initial vector of u_{tot} must be flipped, i.e. the first

entry must become the last one and vice versa. This ensures that at position $x = 0 \text{ m}^1$ we find the last-sampled-in-time u_{tot} . Note that it was assumed a positive x -axis in the downstream direction. Taylor's frozen flow hypothesis constitutes an approximation, and it inevitably introduces an error by assuming that $u(x, t + \tau) \approx u(x, t)$. The error can be quantified by computing the higher-order Taylor terms that are neglected by Taylor's hypothesis.

1.2.2 Correlation Length of the Velocity Signal

The autocorrelation of the fluctuation $u(x)$ was computed through the built-in MATLAB function `autocorr`. The resulting $C(l)$ is shown in Plot B1. It is possible to define the correlation length L_c as the length l such that $C(l) = \frac{1}{e}$: such a length and the corresponding value of $C(L_c) = \frac{1}{e}$ are highlighted in Plot B1.



Plot B: The autocorrelation function.

The correlation length was also estimated by assuming that only the tails of the distribution scale

¹The position of the origin of the frame of reference is irrelevant for the following analysis.

exponentially, i.e. $C(l) \sim \exp(-l/\xi)$. The value of ξ was then determined by linear approximation of the logarithm of $C(l)$, as shown in Plot B2. The result is reported in Table 1. These lengths are approximations of the integral scale, which is given by:

$$L_{int} = \int_0^\infty C(l)dl \quad (6)$$

This integral was numerically computed by integrating with `trapz` the function $C(l)$ between $l = 0$ m and the first value of l for which $C(l)$ crosses the x -axis. This is common practice, since for higher values of l the autocorrelation oscillates around 0.

For the given experimental setup, the integral scale may be defined by the dimension of the fan that moves the flow in the wind tunnel, i.e. the source of energy input into the system. Since the paddles of the fan have a size of approximately 0.1 m, the integral scale should be $l_0 \sim 1 \times 10^{-1}$ m: the obtained values are indeed in line with this estimation. Additionally, both ξ and L_c deviate from the computed values of L_{int} by no more than 7 mm, and can thus be regarded as reliable approximations. In the following, L_c is adopted as the integral length scale l_0 .

1.2.3 Energy Spectrum of the Flow

The energy spectrum of the signal $u(x)$ is defined as:

$$E(k) \equiv \left| \frac{1}{\sqrt{2\pi L}} \int_0^L u(x) e^{-ikx} dx \right|^2 \quad (7)$$

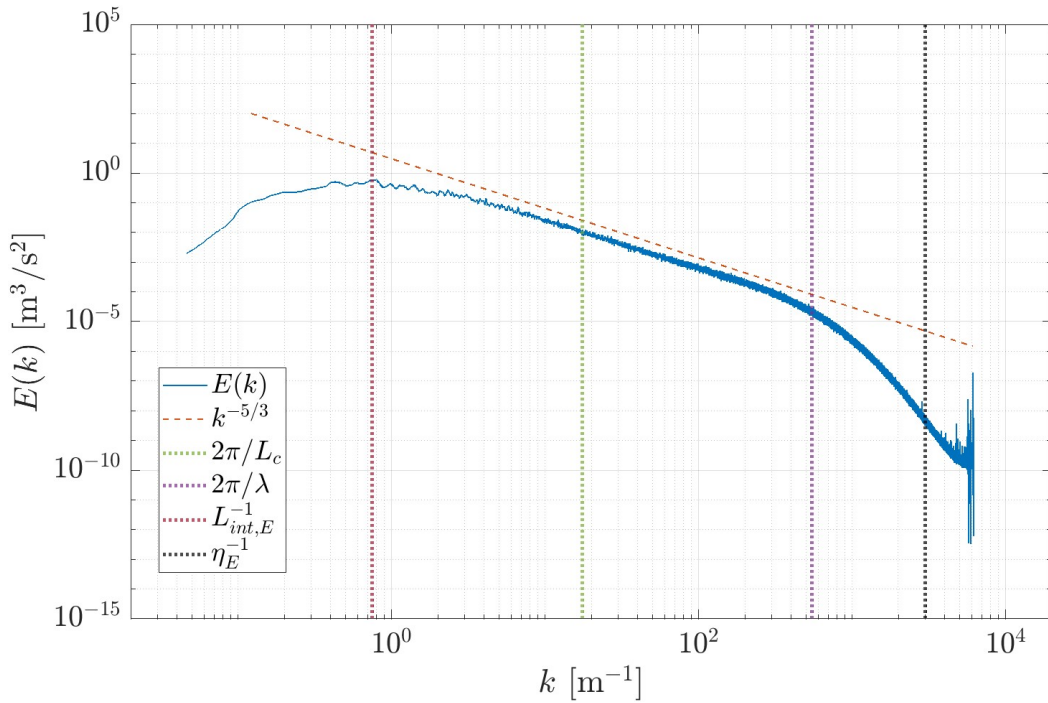
This equation applies to the continuous case. Since we are dealing with a discrete signal $u(x)$, the above expression was evaluated by computing the discrete Fourier transform of $u(x)$ using the built-in command `fft`. The resulting transform is symmetric²: this is the reason why it is possible to move from the definition of the spectral energy density to that of the energy spectrum simply by multiplying the first half of the coefficients of the former by two³. The value of L in Eq. 7 is the largest x -position reached by the array of space positions. In order to minimize the noise, a Butterworth lowpass filter was applied to $E(k)$ after computing the FFT. Plot C shows the resulting energy spectrum: the theoretical slope of $k^{-5/3}$ in the inertial range is plotted as well, along with the values of the approximated integral scale $l_0 = L_c$ and the Taylor length scale λ (see Eq. 9). By visual inspection, it is possible to identify a range of wavenumbers for which $E(k)$ follows the K41 prediction: $L_{int,E}$ and η_E were obtained in this way, and their corresponding wavenumbers are reported in Plot C. In particular $L_{int,E}$ was selected as $\sim k_0^{-1}$, where k_0 is the wavenumber for which the energy spectrum reaches a maximum, while $\eta_E \sim k_{\eta_E}^{-1}$ was taken roughly one decade after the deviation of the energy spectrum from the theoretical prediction⁴. Note that, although the computed value of $l_0 (= L_c)$ does not exactly match $L_{int,E}$, the two values differ only by a factor ≈ 3.5 . Similarly, for $k \sim \lambda^{-1}$, the energy spectrum is still following the K41 prediction: according to K41, λ should identify a wavenumber for which the $-5/3$ scaling is still noticeable. Even this length seems to be consistent with the theoretical results. Finally, the correctness of the normalization was checked using Parseval's theorem:

$$\frac{1}{2} \langle u^2 \rangle = \int_0^\infty E(k) dk \quad (8)$$

²The DFT of a real signal is symmetric. See [3].

³The first entry of the output of `fft` was neglected as well since it is a non-weighted average of the signal.

⁴It can be shown that the deviation takes place for $k \sim \frac{1}{10\eta}$.



Plot C: Energy spectrum. The integral, Taylor and Kolmogorov length scales are highlighted.

The relative error between the LHS and RHS adds up to 7.69×10^{-8} : this value was considered proof of the correctness of the adopted normalization.

1.2.4 The Dissipation Rate and Different Reynolds Numbers

It is possible to compute the Taylor's length scale as follows:

$$\lambda = \sqrt{\frac{15\nu\langle u^2 \rangle}{\varepsilon}} \quad (9)$$

Besides, the value of the energy dissipation rate can be computed as:

$$\varepsilon = \frac{1}{2} \sqrt{\frac{\langle u^2 \rangle^3}{L_c}} \quad (10)$$

The corresponding values are presented in Table 1. The Taylor's length scale is $\lambda = 0.0138$ m. The formulae for Re_λ and the outer Re are the following:

$$Re_\lambda = \frac{\sqrt{\langle u^2 \rangle}\lambda}{\nu} \quad (11)$$

$$Re = \frac{\sqrt{\langle u^2 \rangle}l_0}{\nu} \quad (12)$$

For what concerns the Reynolds number at the Kolmogorov scale, Re_η , this must be equal to 1 since, by definition, η is the scale at which the viscous effects become of the same order of magnitude as the inertial effects. This can be further verified by stating that:

$$Re_\eta = \frac{v_\eta \eta}{\nu} \quad (13)$$

Now, v_η can be estimated as follows:

$$v_\eta \sim \varepsilon^{\frac{1}{3}} \eta^{\frac{1}{3}} \quad (14)$$

while:

$$\eta = \left(\frac{\nu^3}{\varepsilon} \right)^{1/4} \quad (15)$$

Plugging these values in the definition of Re_η immediately yields:

$$Re_\eta = 1 \quad (16)$$

as expected.

1.2.5 Velocity Increments

The longitudinal velocity increment is defined as:

$$\delta u_{||}(x, l) := u(x + l) - u(x) \quad (17)$$

It was computed numerically, given a certain l , by shifting the vector u of the number of indices that make up l , and then the subtraction was computed only where the vectors $u(x+l)$ and $u(x)$ overlapped. As a consequence, the length of the vector associated with $\delta u_{||}(x, l)$ was slightly shrunk with respect to the original length. The trend of $\delta u_{||}(x, l)$ for $l \in \{1 \text{ mm}, 1 \text{ cm}, 10 \text{ cm}, 10 \text{ m}\}$ is shown in Plot D⁵. Note that, as a consequence of the previous discussion, $l = 10 \text{ m}$ lies in the outer range, above the integral scale; $l = 10 \text{ cm}$ and $l = 1 \text{ cm}$ lie in the inertial range and $l = 1 \text{ mm}$ is practically in the dissipation range, since the energy spectrum in Plot C has already deviated from the $-5/3$ scaling for $k \sim 10^3$.

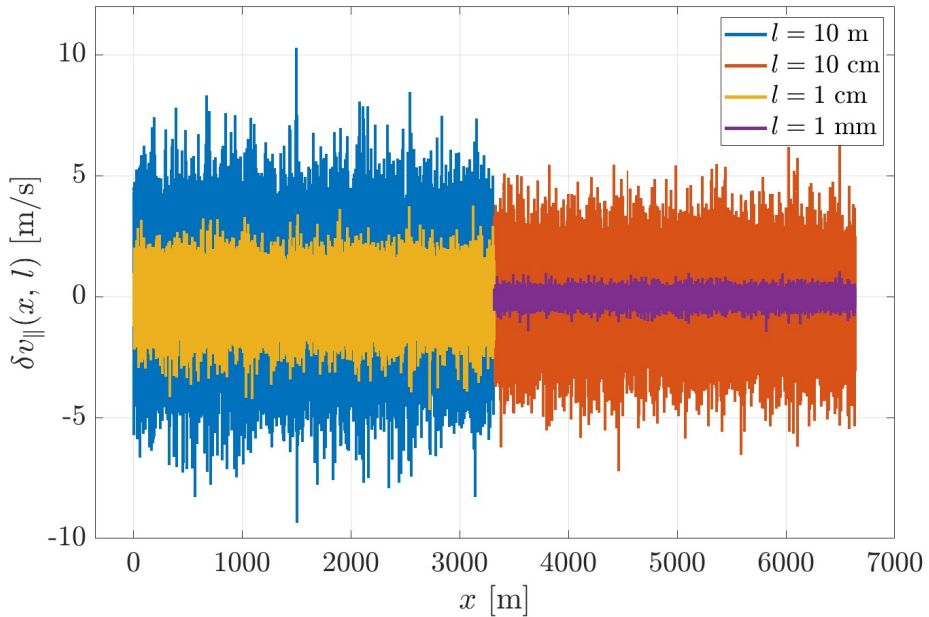
Now, if l increases, we are comparing data far away in space (originally, in time). In light of this, the trend in Plot D comes as no surprise: the more distant the evaluations of $u(x+l)$ and $u(x)$, the more likely they will be different, i.e. the less correlated they will be, as confirmed by the trend of the autocorrelation function $C(l)$ (Plot B1). For $l \gg L_c$, the autocorrelation function tends to zero as $u(x+l)$ and $u(x)$ become uncorrelated. This is well-known by the increasing variance of $\delta u_{||}(x, l)$ for increasing values of l in Plot D.

1.2.6 Statistics of Velocity Increments

The PDFs of the previously obtained velocity increments were estimated by means of a kernel density estimation as implemented in MATLAB by the command `ksdensity`. A normal kernel smoother was adopted to obtain a smoother PDF than the one obtainable using histograms⁶. The result is shown in Plot E1. It is once again possible to observe that, the larger the value of l , the smaller the variance of the corresponding PDF, while the probability density functions remain centered, i.e. zero-mean, for all values of l , and no skewness is noticeable. Additionally, in Plot E2, the estimated PDFs are compared with the Gaussian distributions having the same mean and variance.

⁵For a matter of readability and comparability, only half of each vector is displayed here.

⁶See the [Kernel density estimation](#) page of Wikipedia.



Plot D: Velocity increments for four different values of l .

While for small l the PDFs seem not to match a Gaussian distribution, for $l = 10\text{ m}$ the two curves show a comparable trend in a semilog plot. This can be explained by considering that, for large l , $u(x + l)$ becomes uncorrelated with $u(x)$ and, by the Central limit theorem, the signal $\delta u_{\parallel}(x, l)$ will follow a Gaussian distribution, since it is made of identically distributed independent samples.

1.2.7 Structure Functions and Energy Dissipation

Given the definition of the p -th order structure function:

$$S_p(l) := \langle \delta u_{\parallel}^p(x, l) \rangle \quad (18)$$

Kolmogorov's theory shows, under the assumption of restoration of the symmetries for $Re \rightarrow \infty$ and the finite energy dissipation hypothesis⁷, the validity of both the four-fifths law:

$$\lim_{l \rightarrow 0} \lim_{\nu \rightarrow 0} \lim_{t \rightarrow \infty} \frac{S_3(l)}{l} = -\frac{4}{5}\varepsilon \quad (19)$$

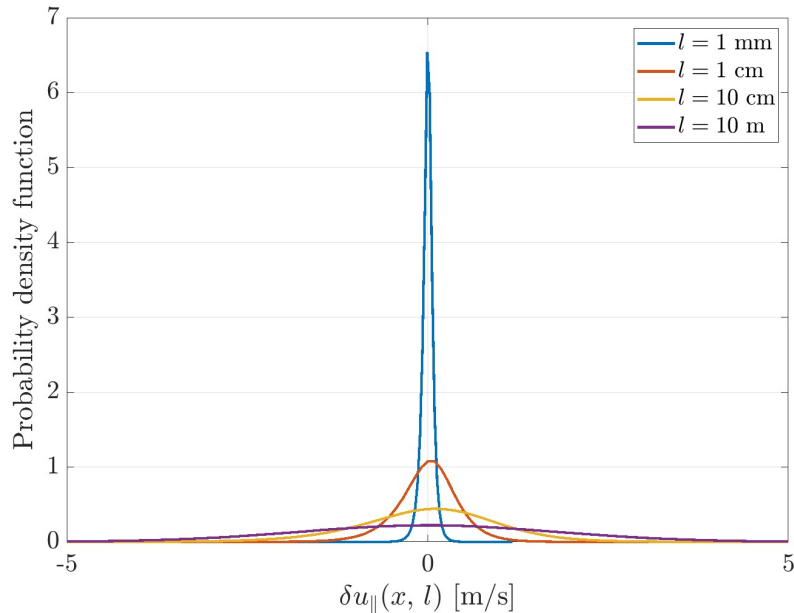
and, assuming also self-similarity⁸, of the following relationship:

$$S_p(l) = C_p \varepsilon^{p/3} l^{p/3} \quad (20)$$

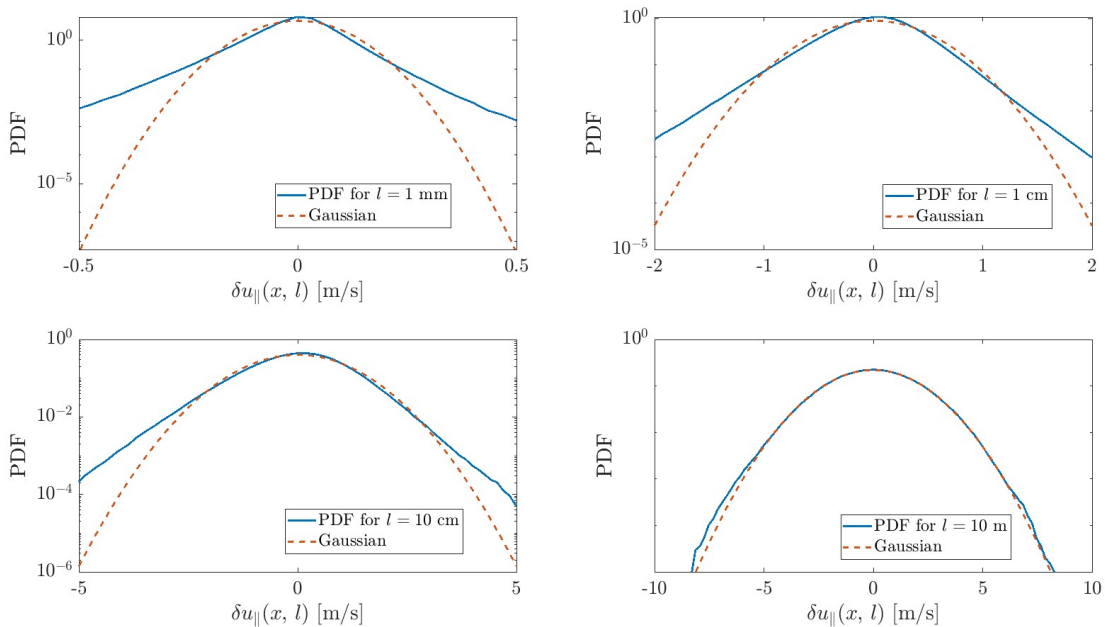
Note that C_2 could be a universal constant ($C_2 \approx 2.1$ according to K. Sreenivasan) even though this is yet to be proven. Plot F shows both $S_2(l)$ and the prediction given by Eq. 20 (dashed line). It is possible to notice a range of l for which the prediction is in line with the experimental results: the lengths for which this happens span from $l \sim 1.5 \times 10^{-2}\text{ m}$ to $l \sim 3 \times 10^{-1}\text{ m}$. These values are consistent with the results obtained studying the energy spectrum: the corresponding wavenumbers individuate indeed a range for which the energy spectrum follows the $k^{-5/3}$ prediction in Plot C, even though the S_2

⁷H1 and H3 as presented in [2].

⁸H2, *ibidem*.



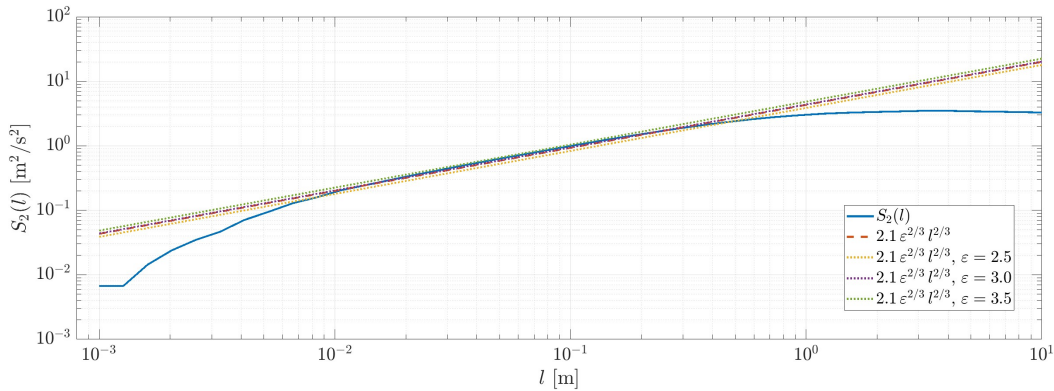
(1) Estimated PDFs for the velocity increments.



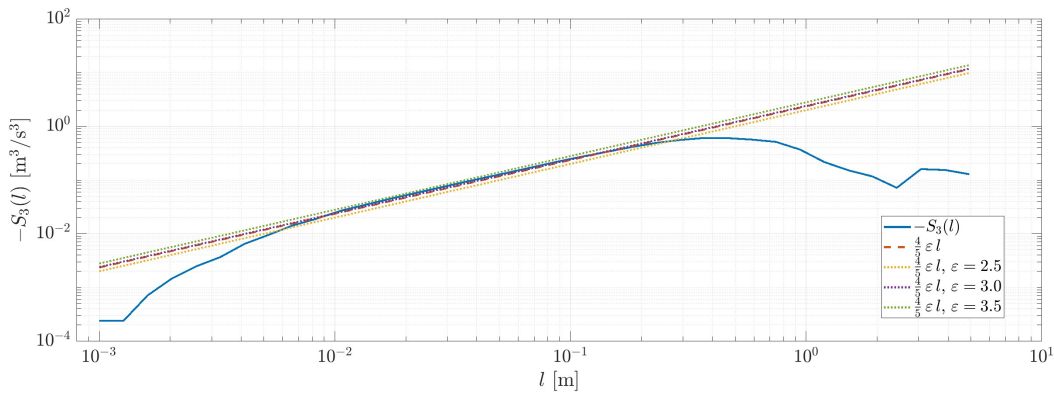
(2) Comparison of the estimated PDFs for $\delta u_{\parallel}(x, l)$ with a Gaussian distribution having the same mean and variance.

Plot E

trend deviates from the K41 scaling law for a larger value of l ($\approx 1.5 \times 10^{-2}$ m against $\approx 2.5 \times 10^{-3}$ m). Additionally, the K41 prediction can be used to estimate the value of ε : in Plot F the power law of $S_2(l)$ is plotted in dotted line for different values of ε . By visual inspection, it seems like $\varepsilon \approx 3 \text{ J}/(\text{kg} \cdot \text{s})$ would fit the experimental data: this value is extremely close to the previously computed $\varepsilon = 2.9405 \text{ J}/(\text{kg} \cdot \text{s})$. Now, thanks to the Wiener-Khinchin formula, if $E(k)$ follows a power law with exponent $-n$ then $S_2 \propto |r' - r|^{n-1}$, and since $n - 1 = 2/3$, we have $n = 5/3$, and it is possible to write:



Plot F: Second order longitudinal structure function.



Plot G: Third order longitudinal structure function.

$$E(k) \sim k^{-5/3} \varepsilon^{2/3} \quad (21)$$

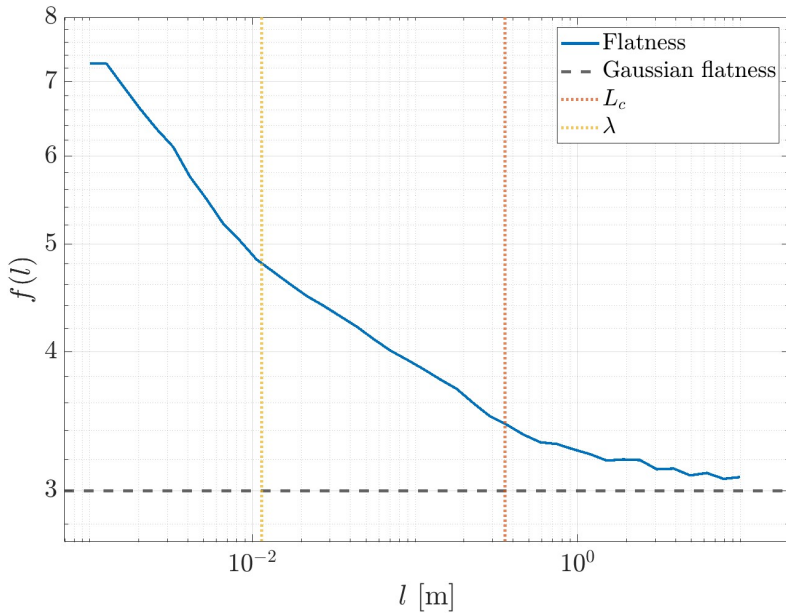
For what concerns $S_3(l)$, Plot G shows its trend, compared with the prediction of the four-fifth law. The range of l for which accordance is observed is similar to the range found looking at $S_2(l)$, although $S_3(l)$ deviates from the K41 prediction for $l \sim 2 \times 10^{-1}$ m, that is, sooner than the $S_2(l)$, but once again these values are in line with the lengths found from the energy spectrum plot. The four-fifth law can be plotted for different values of ε : once again, the value of ε that visually fits the data is very close to the computed one. Besides, in this case, since the four-fifth law is obtained without hypothesis H2, this visual approach may lead to a more confident estimation of ε , especially because the coefficient $C_3 = 4/5$ is known exactly.

1.2.8 Flatness of Velocity Increments

The flatness of the velocity increment signal $\delta u_{\parallel}(x, l)$ is defined as:

$$f(l) = \frac{\langle \delta u_{\parallel}^4(x, l) \rangle}{\langle \delta u_{\parallel}^2(x, l) \rangle^2} \quad (22)$$

By applying its definition, and using the implemented MATLAB function `structure_fct.m`, the flatness $f(l)$ was computed numerically: the result is shown in Plot H.



Plot H: Flatness of the velocity increment. The flatness of a Gaussian distribution is plotted in a black dashed line. Both the estimate of the integral scale L_c and Taylor scale λ are shown as references.

Let us now show that the flatness of a Gaussian distribution equals 3. First of all, we must compute the fourth-order moment:

$$\langle v^4 \rangle = \int_{-\infty}^{\infty} x^4 p(x) dx = \int_{-\infty}^{+\infty} x^4 \frac{1}{\sqrt{2\pi}\sigma} e^{-\frac{x^2}{2\sigma^2}} dx = \int_{-\infty}^{+\infty} x^3 \cdot x \frac{1}{\sqrt{2\pi}\sigma} e^{-\frac{x^2}{2\sigma^2}} dx \quad (23)$$

Such an equation was displayed in this way to emphasize the terms used to apply integration by parts, which yields:

$$\langle v^4 \rangle = \lim_{t \rightarrow \infty} \left[x^3 \left(-\frac{\sigma}{\sqrt{2\pi}} e^{-\frac{x^2}{2\sigma^2}} \right) \right]_{-t}^{+t} + \int_{-\infty}^{+\infty} \frac{3x^2\sigma}{\sqrt{2\pi}} e^{-\frac{x^2}{2\sigma^2}} dx \quad (24)$$

The first term in the RHS vanishes by comparison of the orders of infinity. The remaining term can be once again integrated by parts:

$$\langle v^4 \rangle = \lim_{t \rightarrow \infty} \left[3x \cdot \left(-\frac{\sigma^3}{\sqrt{2\pi}} e^{-\frac{x^2}{2\sigma^2}} \right) \right]_{-t}^{+t} + \int_{-\infty}^{+\infty} \frac{3\sigma^3}{\sqrt{2\pi}} e^{-\frac{x^2}{2\sigma^2}} dx \quad (25)$$

Again, the first term vanishes. In the remaining integral, it is possible to recognize the error function $\text{erf}(x) = \frac{2}{\sqrt{\pi}} \int_0^x e^{-t^2} dt$, barring a prefactor of $3\sigma^4/2$. Since $\lim_{x \rightarrow \pm\infty} \text{erf}(x) = \pm 1$, we have:

$$\langle v^4 \rangle = \frac{3\sigma^4}{2} \cdot 2 = 3\sigma^4 \quad (26)$$

Finally, since the flatness is computed as the ratio of the fourth-order moment to the second-order moment squared, we have:

$$f = \frac{\langle v^4 \rangle}{(\langle v^2 \rangle)^2} = \frac{3\sigma^4}{(\sigma^2)^2} = 3 \quad (27)$$

which shows that the flatness of a Gaussian distribution is constant and equal to 3. Now, as already stated, as l grows the values of $u(x + l)$ and $u(x)$ become uncorrelated, and the velocity increment signal tends to follow a Gaussian distribution according to the Central limit theorem. This is shown by the trend of the flatness: for large l , the flatness tends to be that of a Gaussian distribution. On the contrary, for decreasing l the flatness grows. This is a consequence of the fact that the fluctuations of velocity become correlated, and a non-constant flatness is also possible evidence of intermittency in the inertial range, as discussed in Sec. 1.3. Consequently, the associated PDF has a narrower shape (smaller variance) and a higher peak.

1.2.9 Results Table

Table 1: Table of results

Param.	Dim.	Val.	Param.	Dim.	Val.
U	m/s	1.021×10^1	η_E	m	3.333×10^{-4}
I	-	1.255×10^{-1}	η	m	1.8956×10^{-4}
L_C	m	3.578×10^{-1}	ϵ	J/(kg · s)	2.9405
ξ	m	3.572×10^{-1}	Re_λ	-	9.3905×10^2
L_{int}	m	3.537×10^{-1}	Re	-	2.9394×10^4
$L_{\text{int},E}$	m	1.333	Re_η	-	1

1.3 Discussion

1.3.1 Vanishing viscosity

The entire K41 theory is based on the hypothesis that the considered flow has an infinite Reynolds number. However, the hypothesis of infinite Re cannot be verified in an experimental setup: as a result, it has been shown how the four-fifths law, for instance, has not yet been observed due to the Reynolds number not being sufficiently large [1]. Nevertheless, the results in Plot C as well as Plot F and G show notable accordance of the experimental data with the K41 prediction. In practice, the K41 theory makes a prediction in the range of lengths for which the dissipation is negligible. This is expressed mathematically by considering in the scale-by-scale energy budget the limit $\lim_{\nu \rightarrow 0} 2\nu\Omega_k = 0$ to get to the four-fifth law and, subsequently, to both a general law for $S_p(l)$ and, using the Wiener formula, to the $-5/3$ scaling of the energy spectrum. The whole argument holds true as long as the previous limit can be considered approximately zero: if the considered length scale x guarantees a sufficiently high Re_x , by definition of Reynolds number it means that inertial forces are more relevant than the viscous contribution, and we are thus satisfying this constraint, despite the finiteness of the Reynolds number. Increasing the Re in the experimental setup, will not affect the integral scale l_0 , but will decrease the value of η , according to the scale separation $l_0/\eta \sim Re^{3/4}$. This means that, the higher the Reynolds number, the wider the range over which $E(k)$ follows the $k^{-5/3}$ law. Moreover, Frisch shows that a restoration of the symmetries (H1) takes place for high (and yet finite) Re , while empirically it is possible to show that the energy dissipation behaves in a way consistent with a finite positive limit for ν as small as possible, which meets the requirements of H3. In the presented analysis, the energy spectrum shows a clear scaling for lengths in $\approx [2.5 \times 10^{-3}, 0.3]$ m, while the scaling predicted for $S_2(l)$ can be appreciated in $[1.5 \times 10^{-2}, 0.3]$ m, and that of the four-fifth law is noticeable for $l \in [1.5 \times 10^{-2}, 0.2]$ m. Note that, although $E(k)$ and $S_2(l)$ are practically the Fourier transforms of each other, this does not

imply an identical span of power-law ranges, as observed by M. Nelkin [2]. For what concerns the energy spectrum, its trend follows the theoretical prediction for $k \sim \lambda^{-1}$ and deviates for $k \sim 1/(10\eta)$, as expected from the theory. On the whole, all the mentioned ranges are inside both $[\eta_E, L_{int,E}]$ and $[\eta, L_c]$: in any case, the K41 predictions hold true in the inertial range, that will enlarge for a higher value of Re .

1.3.2 Self-similarity

The self-similarity assumption states that:

$$\delta v(r, \lambda l) \sim \lambda^h \delta v(r, l) \quad (28)$$

with $h = 1/3$ as a result of the four-fifth law. As a consequence, the flatness $f(l)$ should have the following behavior:

$$f(l) = \frac{C_4 \varepsilon^{4/3} l^{4/3}}{(C_2 \varepsilon^{2/3} l^{2/3})^2} = \frac{C_4}{C_2^2} = \text{const} \quad (29)$$

that is, the flatness should no longer depend on l and become constant. The self-similarity is assumed at the scales smaller than the integral scale l_0 , i.e. between $\sim l_0$ down to $\sim \eta$. However, Plot H shows that, in the inertial range, the flatness is not constant (and becomes constant for $l \geq l_0$ as a consequence of the central limit theorem). This opens to a few considerations. On the one hand, it may be evidence of the existence of intermittency in the inertial range. If this was the case, the K41 prediction of $S_2(l)$ and $S_4(l)$ would require an intermittency correction (while the four-fifth law would still hold true), and hence we would have:

$$f(l) \sim l^{\alpha_4 - 2\alpha_2} \quad (30)$$

where α_4 is the correction of the exponent of $S_4(l)$ and α_2 is the correction of the exponent of $S_2(l)$. This consideration would be reasonable if we considered the initial experiment (and the present analysis) to be correctly carried out, and the measurements not to be affected by a relevant error. This kind of assumption is far from verified: not only is our analysis improvable, but the amount of data processed is likely too small to draw conclusions regarding the intermittency. Moreover, these exponents would change the prediction of the scaling of the energy spectrum as well: a continuous trial-and-error approach is required to find suitable exponents.

2 Part II: The chaotic behavior of non-smooth 2D maps

2.1 Analytical study of the map

Given the discrete 2D dynamical system described by the following transformation:

$$\begin{pmatrix} x_{n+1} \\ y_{n+1} \end{pmatrix} = M \begin{pmatrix} x_n \\ y_n \end{pmatrix} \quad \text{mod } N, \quad M = \begin{pmatrix} 1 & 1 \\ ab + 1 & a \end{pmatrix} \quad (31)$$

with $N \in \mathbb{N}$, $a, b \in \mathbb{R}$, and $0 \leq x, y < N$, it is possible to study its characteristics. In particular, its Jacobian J is simply:

$$J \equiv M = \begin{pmatrix} 1 & 1 \\ ab + 1 & a \end{pmatrix} \quad (32)$$

The determinant of the Jacobian is thus:

$$\det J = a - ab - 1 \quad (33)$$

Therefore the map will be dissipative ($|\det J| < 1$) if:

$$a < 0, \quad 1 < b < \frac{a-2}{a} \quad (34)$$

$$a > 0, \quad \frac{a-2}{a} < b < 1 \quad (35)$$

The eigenvalues of J are computed by imposing the condition $\det(J - \mu\mathbb{I}) = 0$, yielding:

$$\mu_{1,2} = \frac{(a+1) \pm \sqrt{a^2 - 2a + 4ab + 5}}{2} \quad (36)$$

The corresponding eigenvectors \mathbf{h}_i are obtained by solving the linear system $(J - \mu_i\mathbb{I})\mathbf{h}_i = 0$. The resulting eigenvectors are⁹:

$$\mathbf{h}_1 = \begin{pmatrix} \frac{2}{(a-1)+\sqrt{a^2-2a+4ab+5}} \\ 1 \end{pmatrix} \quad (37)$$

while for μ_2 we have:

$$\mathbf{h}_2 = \begin{pmatrix} -\frac{2}{(1-a)+\sqrt{a^2-2a+4ab+5}} \\ 1 \end{pmatrix} \quad (38)$$

and all the parallel vectors.

⁹All the vectors parallel to \mathbf{h}_1 are eigenvectors associated with μ_1 .

In order to compute the Lyapunov exponents of the given map, starting from their definition (in discrete time):

$$\lim_{n \rightarrow \infty} \lim_{\|\varepsilon_0\| \rightarrow 0} \frac{1}{n} \ln \left(\frac{\|\varepsilon(n)\|}{\|\varepsilon_0\|} \right) \quad (39)$$

where $\|\cdot\|$ denotes the Euclidean norm. By means of a Taylor expansion up to the first order, the perturbation after n iterations can be approximated as:

$$\varepsilon(n) \approx \left(\prod_{j=0}^{n-1} J \right) \varepsilon_0 \quad (40)$$

Note that, for the given map, the Jacobian does not depend on the current point $[x_n, y_n]^T$. Therefore, Eq. 39 can be rewritten as follows:

$$\lambda \approx \lim_{n \rightarrow \infty} \lim_{\|\varepsilon_0\| \rightarrow 0} \frac{1}{n} \ln \left\| \left(\prod_{j=0}^{n-1} J \right) \hat{\varepsilon}_0 \right\| \quad (41)$$

It is now possible to bring the product out of the logarithm, getting a sum over constant terms: the prefactor $1/n$ can thus be simplified, and if we choose ε to be an eigenvector of J with unit norm we get:

$$\lambda_1 \approx \ln(|\mu_1|) \quad (42)$$

and similarly

$$\lambda_2 \approx \ln(|\mu_2|) \quad (43)$$

2.2 Numerical study of the map

2.2.1 Study-case I ($a = b = 1$)

For $a = b = 1$, the map has the following Jacobian:

$$J = \begin{pmatrix} 1 & 1 \\ 2 & 1 \end{pmatrix} \quad (44)$$

and it can be immediately observed that $\det J = -1$: the map is thus conservative, and we expect two eigenvalues whose sum is zero. We can substitute the values of a and b in Eq. 36-43 in order to get

to:

$$\mu_1 = 1 + \sqrt{2} \quad (45)$$

$$\mu_2 = 1 - \sqrt{2} \quad (46)$$

$$\mathbf{h}_1 = \begin{pmatrix} \frac{\sqrt{2}}{2} \\ 1 \end{pmatrix} \quad (47)$$

$$\mathbf{h}_2 = \begin{pmatrix} -\frac{\sqrt{2}}{2} \\ 1 \end{pmatrix} \quad (48)$$

$$\lambda_1 \sim \ln(|1 + \sqrt{2}|) \approx 0.8814 \quad (49)$$

$$\lambda_2 \sim \ln(|1 - \sqrt{2}|) \approx -0.8814 \quad (50)$$



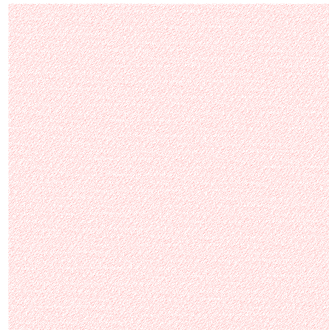
Plot I: Initial condition for study-case I. The image has dimensions 2016×2016 .

It comes as no surprise that there exists an iteration for which the initial condition is met again since the map is conservative. In particular, for the given map, such a restoration takes place at iteration $n = 96$, using as the initial condition the image in Plot I. Additionally, a pattern can be observed among the iterations from $n = 1$ to $n = 96$: for $n = 24$, the initial writing "EPFL" is again vaguely discernible; for $n = 48$, the writing is entirely in the center of the image as shown in Plot J3; for $n = 72$ the image is the same as $n = 24$, and finally for $n = 96$ we get the initial condition. Moreover, the map displays one of the key ingredients for the onset of chaos, i.e. the presence of mixing and topological transitivity, as it can be noticed in Plot J1. The Lyapunov exponents were numerically computed by means of a MATLAB implementation of the map. Plot K1 and Plot K2 show how two initial perturbations parallel to \mathbf{h}_1 and \mathbf{h}_2 evolve. This was exploited to approximate the limit in Eq. 39, which was computed numerically using $\|\varepsilon_0\| = 1 \times 10^{-12}$ and studying the behavior of $\|\varepsilon(n)\|$. The results are the following:

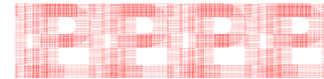
$$\lambda_{1,num} = 0.8814 \quad (51)$$

$$\lambda_{2,num} = -0.8813 \quad (52)$$

A brief discussion about the Lyapunov exponents is necessary to explain how they were approximated. In Eq. 49 and 50 the Lyapunov exponents of the map *without* the modulo operator were computed: it



(1) Iteration $n = 8$



(2) Iteration $n = 24$



(3) Iteration $n = 48$



(4) Iteration $n = 72$

Plot J: Remarkable iterations of the map for the study-case I.

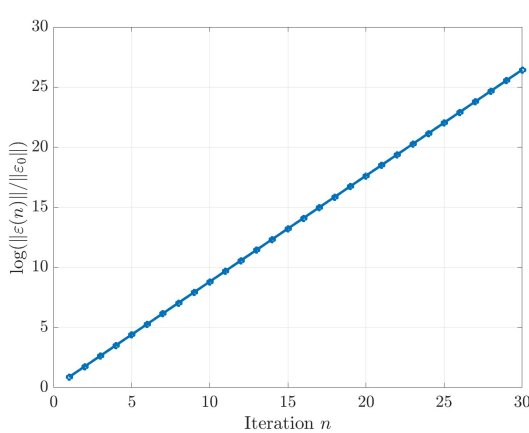
can be shown that this does not affect the computation of the Lyapunov exponent, although no formal proof is provided here. If we do not consider the modulo, we can state that only an initial condition parallel to \mathbf{h}_2 allows the approximation of λ_2 . In such a case, as Plot K2 shows, after a few iterations (roughly 20), the norm of the perturbation $\|\varepsilon(n)\|$ becomes comparable to the $\varepsilon_{\text{machine}}$: the floating point representation of the output of the map is no longer sufficiently accurate, and once again we end up approximating the Lyapunov exponent λ_1 (the slope of the plot becomes positive). Conversely, an initial condition parallel to \mathbf{h}_1 quickly grows in the Euclidean norm, showing the sensitivity to initial conditions of this map, another key ingredient for the emergence of chaos. Finally, for this map, the box-counting dimension D_0 is equal to the number of dimensions of the space in which the map is defined, i.e. $D_0 = 2$. This is a consequence of the fact that this system is conservative: all trajectories can visit the entire 2-dimensional space, and thus the attractor of the system is the space itself.

2.2.2 Study-case II ($a = 3, b = 0.5$)

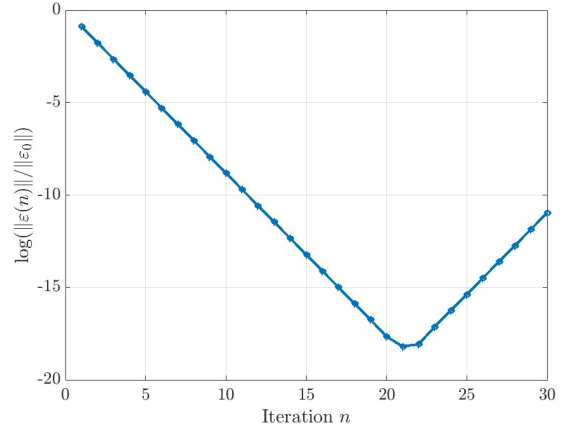
For $a = 3, b = 0.5$, the Jacobian of the map is:

$$J = \begin{pmatrix} 1 & 1 \\ \frac{5}{2} & 3 \end{pmatrix} \quad (53)$$

with $\det J = \frac{1}{2}$. Therefore in this case the map is dissipative: at every iteration, the volume of the



(1) Initial condition parallel to \mathbf{h}_1 .



(2) Initial condition parallel to \mathbf{h}_2 .

Plot K: Numerical approximation of the Lyapunov exponents, study-case I.

system is halved. Besides, we have:

$$\mu_1 = \frac{4 + \sqrt{14}}{2} \quad (54)$$

$$\mu_2 = \frac{4 - \sqrt{14}}{2} \quad (55)$$

$$\mathbf{h}_1 = \begin{pmatrix} \frac{\sqrt{14}-2}{5} \\ 1 \end{pmatrix} \quad (56)$$

$$\mathbf{h}_2 = \begin{pmatrix} -\frac{\sqrt{14}+2}{5} \\ 1 \end{pmatrix} \quad (57)$$

$$\lambda_1 \sim \ln \left| \frac{4 + \sqrt{14}}{2} \right| \approx 1.3535 \quad (58)$$

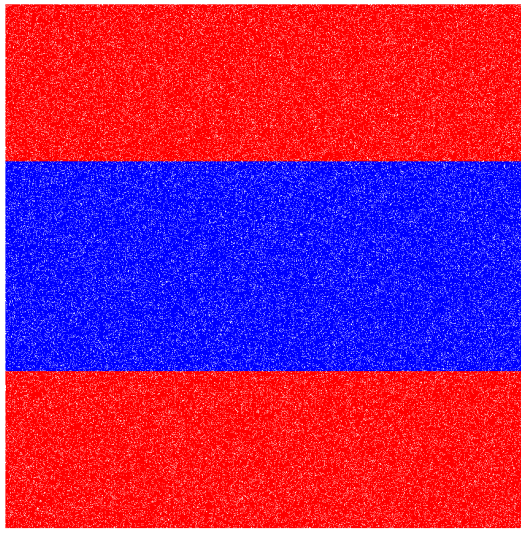
$$\lambda_2 \sim \ln \left| \frac{4 - \sqrt{14}}{2} \right| \approx -2.0466 \quad (59)$$

The initial condition for the numerical study is the one shown in Plot L. This was obtained by creating a grid of $N_p \times N_p$ pixels, and allowing a random number of colored pixels in three stripes, red for $y \in (0, 1.5]$, blue for $y \in [1.5, 3.5]$ and again red for $y \in (3.5, 5]$. In this study-case, x_n and y_n can take any real value in $[0, 5] \times [0, 5]$. That said, their value had to be quantized in order to be able to plot them on a grid of $N_p \times N_p$ number of pixels¹⁰. A look at the first iterations of the map clearly shows that at each iteration there exists an attractor (the visible stripes) of dimension smaller than 2, along which the points tend to align. The same approach presented for the study-case I was adopted to estimate the Lyapunov exponents, yielding:

$$\lambda_{1,num} = 1.3535 \quad (60)$$

$$\lambda_{2,num} = -2.0466 \quad (61)$$

¹⁰The map could have been implemented differently to avoid this quantization, and yet this approach was adopted because it led to more efficient cycling through the points when computing the box-counting dimension.



Plot L: Initial condition for study-case II.

It is possible to note that the numerical approximation matches the more analytical approach up to the fourth significant digit, thus showing the consistency of the adopted procedure.

The box-counting dimension D_0 (Minkowski dimension) can be estimated with an analytical approach following the same reasoning that can be applied to the Cantor set: for the given map, it is possible to note a fractal since at each iteration, each colored stripes is divided in 8 stripes, 4 of which become white. Hence, if we denote with D_x the box-counting dimension in the direction parallel to the stripes and D_y the box-counting dimension in the direction orthogonal to the stripes, we get:

$$D_0 = D_x + D_y = 1 + \frac{\log 4}{\log 8} \approx 1.667 \quad (62)$$

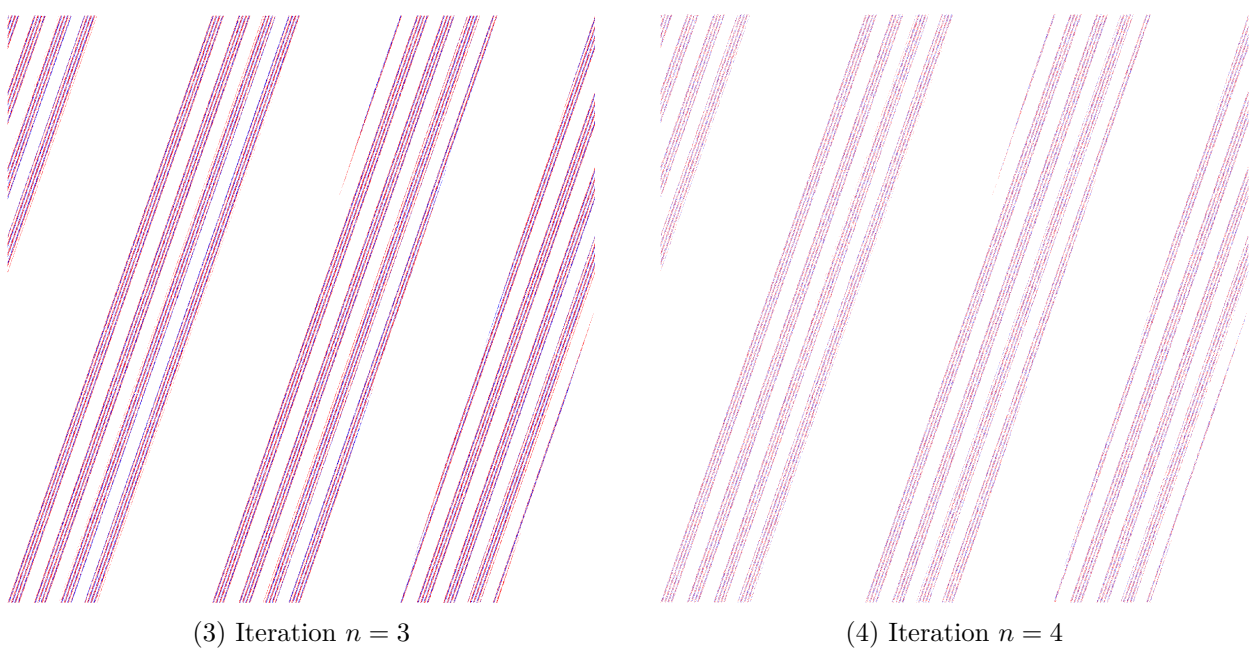
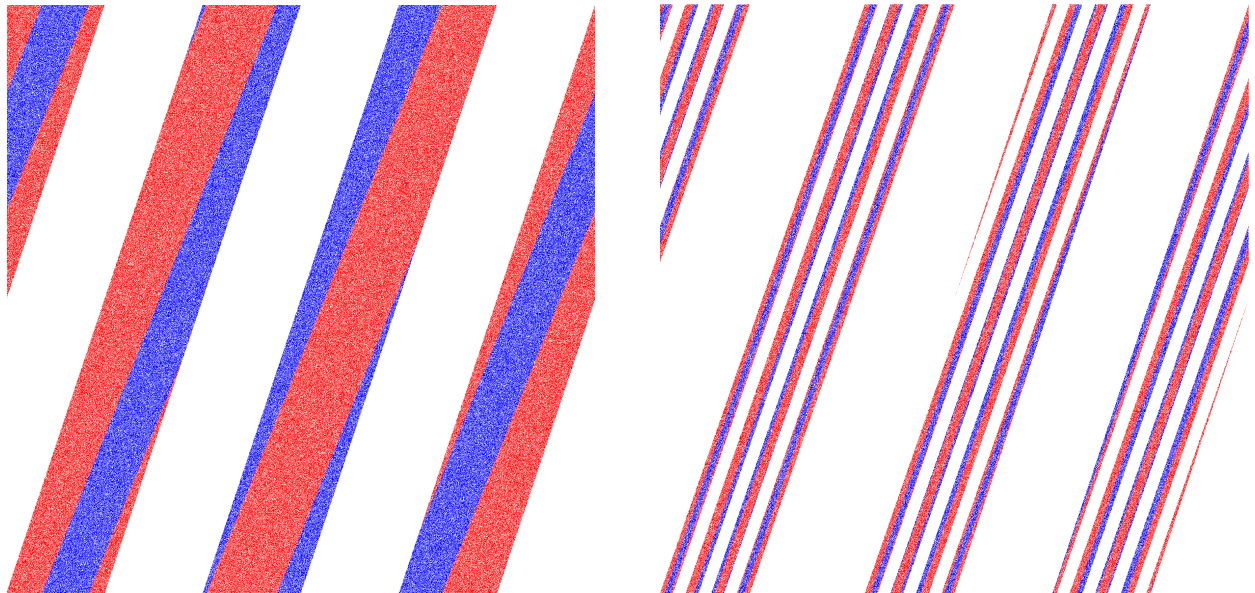
A MATLAB function `box_counting.m` was implemented to compute the same quantity numerically, according to its definition:

$$D_0 = \lim_{r \rightarrow 0} \frac{\ln(N(r))}{\ln(1/r)} \quad (63)$$

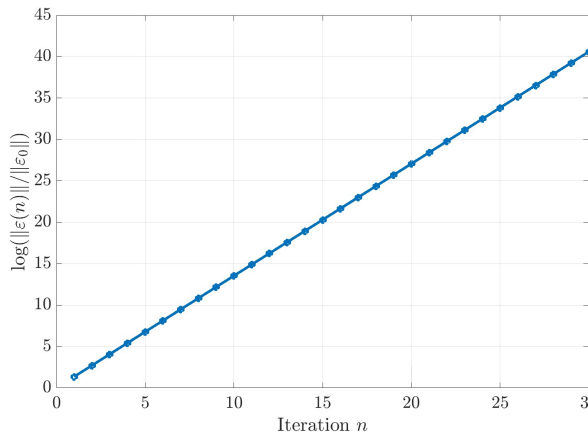
where r is the side length of the boxes used to decompose the space and $N(r)$ the number of occupied boxes. The computation was carried out for iteration $n = 5$. For $N_p = 4096$, the grid was divided into a number of boxes each time squared: 2^{2k} boxes, with $k = 1, \dots, 12$. Then, the number of non-empty boxes was evaluated cyclically. The result is shown in Plot O. Numerically it is not possible to exactly have the convergence of the box-counting dimension since no more than $N_p \times N_p$ boxes can be created. That said, the plot shows that D_0 indeed tends to the value predicted analytically.

2.3 Discussion

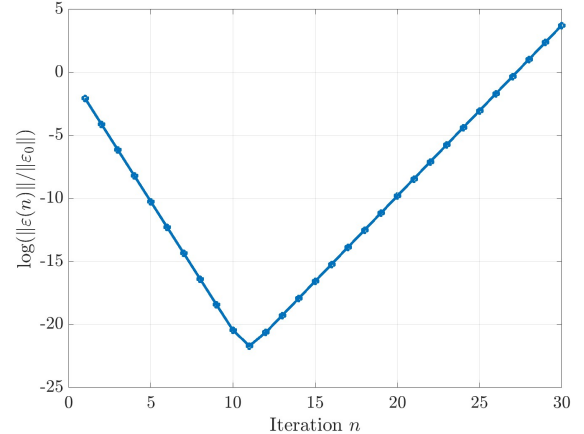
Two different 2D non-smooth maps were studied, each of them having peculiar characteristics. Both maps have at least one positive Lyapunov exponent, and thus the necessary condition for the onset of chaos was fulfilled. In the first case, a conservative chaotic map was studied: it was possible to show



Plot M: First 4 iterations of the map, study-case II. Note the emergence of a fractal.

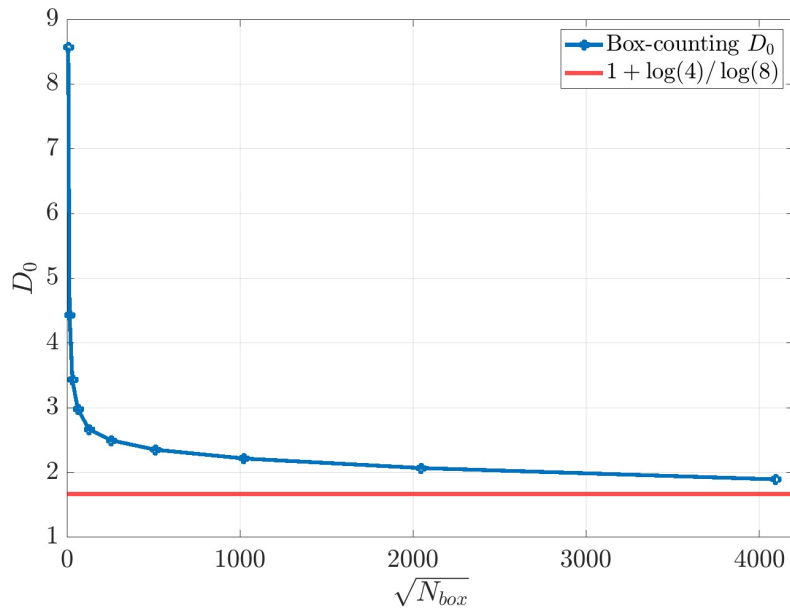


(1) Initial condition parallel to \mathbf{h}_1 .



(2) Initial condition parallel to \mathbf{h}_2 .

Plot N: Numerical approximation of the Lyapunov exponents, study-case II.



Plot O: Numerical computation of the box-counting dimension, study-case II.

that an initial condition is actually restored after $n = 96$ iterations, despite being affected by mixing for many iterations. In the second study case, it was possible to observe the presence of a fractal: at each iteration, the same pattern was discernible when forming new stripes of colored points. Finally, while in the first map the box-counting dimension equals the number of dimensions of the state space, the second map has an attractor: this was also shown by computing the Minkowski dimension of both maps, analytically and numerically. In conclusion, it is possible to see how the deterministic nature of both maps is no hindrance to the emergence of chaotic behavior.

Appendix

References

- [1] R. A. Antonia, S. L. Tang, L. Djenidi, and Y. Zhou. Finite reynolds number effect and the 4/5 law. *Phys. Rev. Fluids*, 4:084602, Aug 2019. doi: 10.1103/PhysRevFluids.4.084602. URL <https://link.aps.org/doi/10.1103/PhysRevFluids.4.084602>.
- [2] U. Frisch and A.N. Kolmogorov. *Turbulence: The Legacy of A. N. Kolmogorov*. Cambridge University Press, 1995. ISBN 9780521457132. URL <https://books.google.ch/books?id=K-Pf7RuYkf0C>.
- [3] P. Prandoni and M. Vetterli. *Signal Processing for Communications*. Communication Sciences. CRC Press, 2008. ISBN 9782940222209. URL <https://books.google.ch/books?id=25XmDAAAQBAJ>.

List of Collaborators

Nicolò Giosuè Carlo Viscusi

Matteo Cirillo

Filippo Brignolo

Personal Statement

I hereby certify that I fully respect the stated Honor Code and specifically that:

1. My report is my original work prepared solely by me;
2. All sources used are cited;
3. All people I collaborated with are listed.

Signature (Francesco Sala)

Date